machines

Article

Enhanced Reaching-Law-Based Discrete-Time Terminal Sliding Mode Current Control of a Six-Phase Induction Motor

Yassine Kali [1], Jorge Rodas [2,*], Jesus Doval-Gandoy [3], Magno Ayala [2] and Osvaldo Gonzalez [2]

[1] Power Electronics and Industrial Control Research Group (GRÉPCI), École de Technologie Supérieure, Montreal, QC H3C 1K3, Canada
[2] Laboratory of Power and Control Systems (LSPyC), Departamento de Ingeniería Electrónica y Mecatrónica (DIEM), Facultad de Ingeniería, Universidad Nacional de Asunción, Luque 2060, Paraguay
[3] Applied Power Electronics Technology Research Group (APET), Universidad de Vigo, 36310 Vigo, Spain
* Corresponding author: jrodas@ing.una.py

Abstract: This paper develops an inner stator current controller based on an enhanced reaching-law-based discrete-time terminal sliding mode. The problem of tracking stator currents with high accuracy while ensuring the robustness of a six-phase induction motor in the presence of uncertain electrical parameters and unmeasurable states is tackled. The unknown dynamics are approximated by using a time delay estimation method. Then, an enhanced power-reaching law is used to make each stage of the convergence faster. A stability analysis and the system controller's finite-time convergence are demonstrated in detail. Practical work was conducted on an asymmetrical six-phase induction machine to illustrate the developed discrete approach's robustness and effectiveness.

Keywords: current control; induction motor; multiphase machine; power-reaching law; sliding mode

check for updates

Citation: Kali, Y.; Rodas, J.; Doval-Gandoy, J.; Ayala, M.; Gonzalez, O. Enhanced Reaching-Law-Based Discrete-Time Terminal Sliding Mode Current Control of a Six-Phase Induction Motor. *Machines* **2023**, *11*, 107. https://doi.org/10.3390/machines11010107

Academic Editors: Antonio J. Marques Cardoso and Rong-Jong Wai

Received: 31 October 2022
Revised: 9 January 2023
Accepted: 11 January 2023
Published: 13 January 2023

1. Introduction

Multiphase motors with a number of phases greater than three have recently been involved in high-power and high-reliability real-life implementations, such as in electric vehicles, ship propulsion, and wind energy conversion systems [1,2]. Their innate fault-tolerant abilities without needing extra hardware are still considered their most practical benefit [3]. Moreover, their additional degrees of freedom have opened the window for miscellaneous nontraditional objectives at the expense of the need for more advanced control strategies [4]. For that reason, a myriad of papers are now available regarding the implementation of control techniques for multiphase machines, and these range from classic controllers (field-oriented control and direct torque control) to more sophisticated ones (model predictive control (MPC) and sliding mode control (SMC)) [5,6].

Finite-control-set MPC (FCS-MPC) is one of the multiphase machines' most popular control techniques [7]. FCS-MPC is typically implemented as predictive torque control or predictive current control in the inner control loop of field-oriented control [8,9]. Its fast dynamic response and easy inclusion of constraints are the main advantages of FCS-MPC [10]. Nevertheless, it suffers from an elevated computational load and highly depends on the accuracy of the system's model. Recently, it has been shown that the discrete-time SMC (DSMC) is a good alternative due to its robustness, fast dynamic response, and lack of a need for high computational requirements [11].

The application of DSMC to multiphase machines not only requires the regulation of multiple planes, namely, $\alpha - \beta$ and $x - y$ for the five- and six-phase cases, but its main drawbacks, i.e., the chattering phenomenon, must be reduced. For that purpose, in [12], DSMC was combined with the exponential reaching law (ERL), and a reasonable reduction of chattering was obtained. Moreover, several reaching law approaches have been proposed for discrete systems [13]. A novel reaching law based on the combination of the power reaching law (PRL) and the ERL was used in [14,15], and an application on a piezoelectric actuator was proposed. This proposition aimed to ensure a smaller width of the quasi-sliding mode compared with that of Gao's classical reaching law [16].

However, the chattering phenomenon still needs to be eliminated when fast responses are required. In addition, the convergence of the selected surface to zero is very slow when the error value is high. To overcome this problem, an exponential-based bi-power reaching law was proposed in [17] and applied experimentally on a voltage source inverter. However, the convergence time was established only for continuous systems and could not reflect the case of a discrete-time system. In [18,19], a super-twisting-like reaching law was developed for a multiphase induction machine. The results obtained in practical work showed good results under parameter mismatch. However, results with a low frequency and high rotor speed showed high chattering activity. In addition, the super-twisting-like algorithm had a low rate speed when the system's states were far away from the designed switching function.

In this paper, a combination of Gao's reaching law and the exponential-based bi-power reaching-law-based discrete-time terminal SMC (DTSMC) with time delay estimation (TDE) is proposed and applied to a six-phase induction motor. The proposed reaching law aims to enhance the reaching rate and reduce the chattering while ensuring a small quasi-sliding mode band. Indeed, each power-reaching law has a different exponent. The first one will take the lead when the system's trajectories are far from the sliding surface and, when added to Gao's reaching law, will ensure a faster convergence rate. The second one will take the lead when the system's trajectories are near the sliding surface to enhance the convergence compared to Gao's reaching law and the classical power-reaching law. Moreover, a terminal sliding surface [19–21] will be adopted instead of a conventional one for faster convergence during the quasi-sliding mode. For robustness issues, the discrete-time TDE [22] is used to estimate the external perturbations and the rotor currents that are unavailable for measurements. A detailed stability study will be presented for the closed-loop error dynamics. The developed discrete-time approach in this paper can be easily extended to any electrical machine. Finally, the developed method was implemented on a real six-phase induction motor.

The rest of this paper is divided as follows. Section 2 details the mathematical model of the system. It comprises a six-phase IM and a power-electronic converter. The proposed current controller is presented in Section 3. A stability analysis is shown in the same section. Then, the real-time validation of the controller is demonstrated in Section 4. The last section summarizes the main aspects of this article.

2. System Modelling

Consider an asymmetrical six-phase IM drive powered by two two-level voltage source converters (2L-VSCs), as shown in Figure 1), with the model [18] given by:

$$\begin{aligned}
\dot{I}_{r\alpha} &= -\frac{CL_sR_r}{L_m}I_{r\alpha} - \frac{CL_sL_r}{L_m}P\omega_m I_{r\beta} + CR_sI_{s\alpha} - CL_sP\omega_m I_{s\beta} - CU_{s\alpha},\\
\dot{I}_{r\beta} &= \frac{CL_sL_r}{L_m}P\omega_m I_{\alpha r} - \frac{CL_sR_r}{L_m}I_{\beta r} + CL_sP\omega_m I_{\alpha s} + CR_sI_{\beta s} - CU_{s\beta},\\
\dot{I}_{s\alpha} &= CR_rI_{r\alpha} + CL_rP\omega_m I_{r\beta} - \frac{CR_sL_r}{L_m}I_{s\alpha} + CL_mP\omega_m I_{s\beta} + \frac{CL_r}{L_m}U_{s\alpha} + d_\alpha,\\
\dot{I}_{s\beta} &= -CL_rP\omega_m I_{r\alpha} + CR_rI_{r\beta} - CL_mP\omega_m I_{s\alpha} - \frac{CR_sL_r}{L_m}I_{s\beta} + \frac{CL_r}{L_m}U_{s\beta} + d_\beta,\\
\dot{I}_{sx} &= \frac{1}{L_{ls}}(-R_sI_{sx} + U_{sx}) + d_x,\\
\dot{I}_{sy} &= \frac{1}{L_{ls}}(-R_sI_{sy} + U_{sy}) + d_y,
\end{aligned} \tag{1}$$

where:

- $I_{r\{\alpha,\beta\}}$ are the unmeasurable rotor currents,
- $I_{s\{\alpha,\beta,x,y\}}$ are the stator currents,
- $U_{s\{\alpha,\beta,x,y\}}$ are the stator input voltages,
- $d_{\{\alpha,\beta,x,y\}}$ are the uncertain dynamics caused by uncertain parameters and the disturbances acting on the stator currents,
- $C = \dfrac{L_m}{L_r L_s - L_m^2}$,
- L_s is the inductance of the stator,
- L_{ls} is the leakage inductance of the stator,
- L_r is the inductance of the rotor,
- R_s and R_r are, respectively, the resistances of the stator and the rotor,
- P is the number of pole pairs,
- ω_m is the mechanical speed,
- ω_r is the rotor's electrical speed,

$$T_e = 3P\left(\psi_{s\alpha} I_{s\beta} - \psi_{s\beta} I_{s\alpha}\right), \tag{2}$$

$$J\dot{\omega}_m + B\omega_m = (T_e - T_L), \tag{3}$$

$$\omega_m = \frac{\omega_r}{P}, \tag{4}$$

T_e is the generated torque, T_L is the load torque, B and J are the coefficients of the friction and the inertia, and $\psi_{s\alpha}$, $\psi_{s\beta}$ are the stator fluxes.

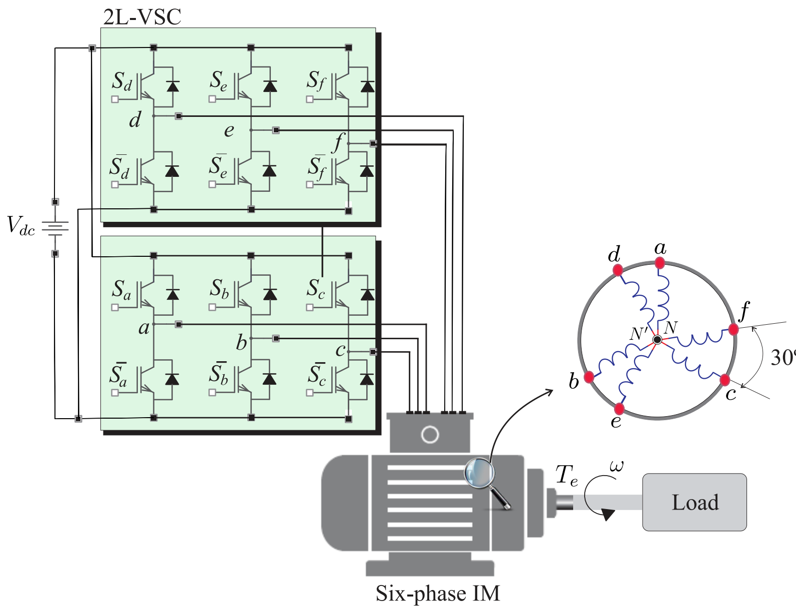

Figure 1. Schematic of the 2L-VSCs and the six-phase IM in an asymmetrical configuration.

With some abuse of notation such that $\bullet_{[n]} = \bullet_{[nT_s]}$ with T_s is a sufficiently small sampling period, the discrete-time model of (1) is obtained:

$$\mathbf{Z}_{[n+1]} = \mathbf{A}_{[n]} + \mathbf{F}_{[n]} + \mathbf{B}\,\mathbf{U}_{[n]}, \tag{5}$$

where:

$$\mathbf{Z}_{[n]} = \left[I_{s\alpha[n]},\, I_{s\beta[n]},\, I_{sx[n]},\, I_{sy[n]}\right]^T, \tag{6}$$

$$\mathbf{A}_{[n]} = \begin{bmatrix} \left(1 - Ts\dfrac{CL_r}{L_m}R_s\right) I_{s\alpha[n]} + T_s CL_m P\omega_{m[n]} I_{s\beta[n]} \\ -T_s CL_m P\omega_{m[n]} I_{s\alpha[n]} + \left(1 - T_s\dfrac{CL_r}{L_m}R_s\right) I_{s\beta[n]} \\ \left(1 - T_s\dfrac{R_s}{L_{ls}}\right) I_{sx[n]} \\ \left(1 - T_s\dfrac{R_s}{L_{ls}}\right) I_{sy[n]} \end{bmatrix}, \tag{7}$$

$$\mathbf{F}_{[n]} = T_s \begin{bmatrix} CR_r I_{r\alpha[n]} + CL_r P\omega_{m[n]} I_{r\beta[n]} + d_\alpha \\ -CL_r P\omega_{m[n]} I_{r\alpha[n]} + CR_r I_{r\beta[n]} + d_\beta \\ d_x \\ d_y \end{bmatrix}, \tag{8}$$

$$\mathbf{B} = T_s \begin{bmatrix} \dfrac{CL_r}{L_m} & 0 & 0 & 0 \\ 0 & \dfrac{CL_r}{L_m} & 0 & 0 \\ 0 & 0 & \dfrac{1}{L_{ls}} & 0 \\ 0 & 0 & 0 & \dfrac{1}{L_{ls}} \end{bmatrix}, \tag{9}$$

$$\mathbf{U}_{[n]} = \left[U_{s\alpha[n]}, U_{s\beta[n]}, U_{sx[n]}, U_{sy[n]}\right]^T. \tag{10}$$

It is worth mentioning that $F_{i[n]} = O(T_s)$ for $i = 1, \cdots, n$ is of the order of one with respect to the sampling time, and this verifies $|F_{i[n]}| \leq T_s \Delta f_i < \infty$. The above assumption is valid for limited speeds and currents and represents the limitations of uncertainties that can be tolerated by the controlled system. Moreover, it should be noted that the rejection of unbounded uncertainties is impossible because it results in such a high control effort that the control signal no longer has any physical meaning.

Otherwise, the input vector is linked to the two-2L-VSC model as follows:

$$\mathbf{U}_{[n]} = V_{\mathrm{dc}} \underbrace{\begin{bmatrix} \frac{1}{3} & \frac{\sqrt{3}}{6} & -\frac{1}{6} & -\frac{\sqrt{3}}{6} & -\frac{1}{6} & 0 \\ 0 & \frac{1}{2} & \frac{\sqrt{3}}{6} & \frac{1}{6} & -\frac{\sqrt{3}}{6} & -\frac{1}{3} \\ \frac{1}{3} & -\frac{\sqrt{3}}{6} & -\frac{1}{6} & \frac{\sqrt{3}}{6} & -\frac{1}{6} & 0 \\ 0 & \frac{1}{2} & -\frac{\sqrt{3}}{6} & \frac{1}{6} & \frac{\sqrt{3}}{6} & -\frac{1}{3} \\ \frac{1}{3} & 0 & \frac{1}{3} & 0 & \frac{1}{3} & 0 \\ 0 & \frac{1}{3} & 0 & \frac{1}{3} & 0 & \frac{1}{3} \end{bmatrix}}_{\mathbf{T}_6} \underbrace{\begin{bmatrix} \frac{2}{3} & 0 & -\frac{1}{3} & 0 & -\frac{1}{3} & 0 \\ 0 & \frac{2}{3} & 0 & -\frac{1}{3} & 0 & -\frac{1}{3} \\ -\frac{1}{3} & 0 & \frac{2}{3} & 0 & -\frac{1}{3} & 0 \\ 0 & -\frac{1}{3} & 0 & \frac{2}{3} & 0 & -\frac{1}{3} \\ -\frac{1}{3} & 0 & -\frac{1}{3} & 0 & \frac{2}{3} & 0 \\ 0 & -\frac{1}{3} & 0 & -\frac{1}{3} & 0 & \frac{2}{3} \end{bmatrix} \begin{bmatrix} S_a \\ S_b \\ S_c \\ S_d \\ S_e \\ S_f \end{bmatrix}}_{\mathbf{M}}, \tag{11}$$

where V_{dc} is the DC-bus voltage, $\mathbf{T}_6$ is the transformation matrix used to obtain (1), and $\mathbf{M}$ is the VSC model, with $S_{\{a,b,c,d,e,f\}}$ denoting the gating signals that switch between 0 and 1.

3. Proposed Discrete-Current Controller Conception

3.1. Outer Control Loop

The aim of this part is to regulate the mechanical speed. In other words, a PI controller will be used:

$$I^r_{sq[n]} = K_P\left(\omega^r_{m[n]} - \omega_{m[n]}\right) + T_s K_I \sum_{j=0}^{n} \left(\omega^r_{m[j]} - \omega_{m[j]}\right). \tag{12}$$

The output of the discrete PI regulator controller used represents the dynamic current reference $I^r_{sq[n]}$ that is used with the imposed $I^r_{sd[n]}$ to compute the $\alpha - \beta$ stator current references (as shown in Figure 2) by using the inverse Park rotating transformation (13) and the indirect estimation of the standard field-oriented control (14) of the rotor flux vector position θ.

$$\begin{bmatrix} I^r_{s\alpha[n]} \\ I^r_{s\beta[n]} \end{bmatrix} = \underbrace{\begin{bmatrix} \cos\theta & -\sin\theta \\ \sin\theta & \cos\theta \end{bmatrix}}_{\mathbf{T}^{-1}_{dq}} \begin{bmatrix} I^r_{sd[n]} \\ I^r_{sq[n]} \end{bmatrix} \tag{13}$$

$$\theta = \int \left(\omega_{r[n]} + \frac{I^r_{sq[n]}}{\tau_r\, I^r_{sd[n]}} \right) dt \tag{14}$$

where $\omega_{r[n]}$ is the rotor speed and τ_r is the rotor time constant. Note that (14) depends on the rotor time constant ($\tau_r = L_r/R_r$), and this parameter varies with temperature. Therefore, as τ_r can change with environmental conditions to calculate θ, it can lead to inefficient control, which is one of the drawbacks of using this estimation technique [23].

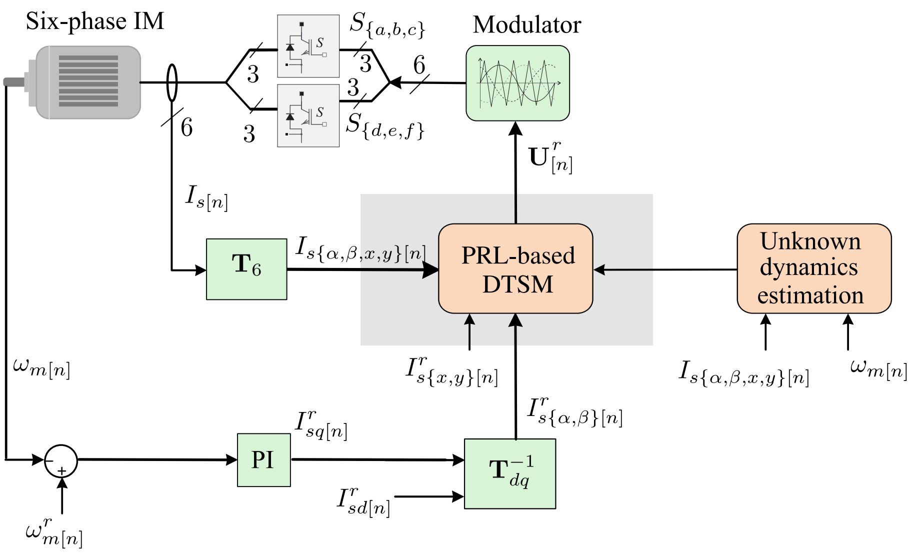

Figure 2. Proposed control scheme.

3.2. Inner Control Loop

In this subsection, a robust current controller based on an enhanced PRL-based DTSMC that is able to reject the effects of unknown dynamics (i.e., the unmeasurable rotor currents $I_{r\{\alpha,\beta\}}$) will be developed to guarantee the accurate tracking of stator currents $I_{s\{\alpha,\beta,x,y\}}$.

First of all, the following discrete-time terminal switching function proposed in [19] is designed:

$$\mathbf{S}_{[n]} = \mathbf{E}_{[n]} + \mathbf{\Lambda}_1 \mathbf{E}_{[n-1]} + \mathbf{\Lambda}_2 \lfloor \mathbf{E}_{[n-1]} \rceil^{\alpha}. \tag{15}$$

where

- $\mathbf{E}_{[n]} = \mathbf{Z}^r_{[n]} - \mathbf{Z}_{[n]}$ is the vector of stator current tracking errors;
- $\mathbf{Z}^r_{[n]} = \left[I^r_{s\alpha[n]}, I^r_{s\beta[n]}, I^r_{sx[n]}, I^r_{sy[n]} \right]^T$ is the vector of stator current references;
- $\mathbf{\Lambda}_1 = \mathrm{diag}(\lambda_{11}, \cdots, \lambda_{14})$ and $\mathbf{\Lambda}_2 = \mathrm{diag}(\lambda_{21}, \cdots, \lambda_{24})$ are diagonal matrices with positive elements;
- $\lfloor \mathbf{E}_{[n-1]} \rceil^{\alpha} = \left[|E_{1[n-1]}|^{\alpha_1} \mathrm{sign}\left(E_{1[n-1]}\right), \cdots, |E_{4[n-1]}|^{\alpha_4} \mathrm{sign}\left(E_{4[n-1]}\right) \right]^T$ where $\alpha_i \in (0,1)$ for $i = 1, \cdots, 4$, and:

$$\mathrm{sign}(E_{i[n]}) = \begin{cases} 0, & \text{if } E_{i[n]} = 0 \\ -1, & \text{if } E_{i[n]} < 0 \\ 1, & \text{if } E_{i[n]} > 0 \end{cases} \tag{16}$$

Secondly, the proposed enhanced PRL-based DTSMC reaching law is given by:

$$\mathbf{S}_{[n+1]} = (\mathbf{I}_4 - T_s\mathbf{L})\mathbf{S}_{[n]} - T_s\mathbf{Q}_1\lfloor\mathbf{S}_{[n]}\rceil^{\gamma_1} - T_s\mathbf{Q}_2\lfloor\mathbf{S}_{[n]}\rceil^{\gamma_2} - T_s\mathbf{Q}_3\lfloor\mathbf{S}_{[n]}\rceil^{0}, \tag{17}$$

- $\mathbf{I}_4$ is the (4×4) identity matrix;
- $\mathbf{L} = \mathrm{diag}(l_1, \cdots, l_4)$, where $l_i > 0$ for $i = 1, \cdots, 4$;
- $\mathbf{Q}_1 = \mathrm{diag}(q_{11}, \cdots, q_{14})$, $\mathbf{Q}_2 = \mathrm{diag}(q_{21}, \cdots, q_{24})$ and $\mathbf{Q}_3 = \mathrm{diag}(q_{31}, \cdots, q_{34})$ are diagonal positive-definite matrices that will be fixed in the proof of stability;
- $\lfloor\mathbf{S}_{[n]}\rceil^{\gamma_k} = \left[|S_{1[n]}|^{\gamma_{k1}}\mathrm{sign}\left(S_{1[n]}\right), \cdots, |S_{4[n]}|^{\gamma_{k4}}\mathrm{sign}\left(S_{4[n]}\right)\right]^T$ for $k = 1,2$ with $\gamma_{1i} \in (0,1)$, $\gamma_{2i} > 1$ for $i = 1, \cdots, 4$, and, finally, $\lfloor\mathbf{S}_{[n]}\rceil^0 = \left[\mathrm{sign}\left(S_{1[n]}\right), \cdots, \mathrm{sign}\left(S_{4[n]}\right)\right]^T$.

On one hand, notice that, in addition to the term $\mathbf{Q}_3\lfloor\mathbf{S}_{[n]}\rceil^0$, the term $\mathbf{Q}_1\lfloor\mathbf{S}_{[n]}\rceil^{\gamma_1}$ takes the lead when the trajectories of the system are near the switching surface $\|\mathbf{S}_{[n]} < 1\|$ to ensure faster convergence. On the other hand, when the trajectories of the system are far away from the switching surface $\|\mathbf{S}_{[n]} \geq 1\|$, the term $\mathbf{Q}_2\lfloor\mathbf{S}_{[n]}\rceil^{\gamma_2}$ takes the lead, making the convergence faster when added to the term $\mathbf{Q}_3\lfloor\mathbf{S}_{[n]}\rceil^0$ in comparison with the known power-reaching law.

To find the expression of the discrete-time control law, let us compute $\mathbf{S}_{[n+1]}$ by using the known parts of the dynamics and the estimation of the unknown parts:

$$\begin{aligned}\mathbf{S}_{[n+1]} &= \mathbf{E}_{[n+1]} + \mathbf{\Lambda}_1\mathbf{E}_{[n]} + \mathbf{\Lambda}_2\lfloor\mathbf{E}_{[n]}\rceil^{\alpha} \\ &= \mathbf{Z}^r_{[n+1]} - \mathbf{Z}_{[n+1]} + \mathbf{\Lambda}_1\mathbf{E}_{[n]} + \mathbf{\Lambda}_2\lfloor\mathbf{E}_{[n]}\rceil^{\alpha} \\ &= \mathbf{Z}^r_{[n+1]} - \mathbf{A}_{[n]} - \hat{\mathbf{F}}_{[n]} - \mathbf{B}\,\mathbf{U}_{[n]} + \mathbf{\Lambda}_1\mathbf{E}_{[n]} + \mathbf{\Lambda}_2\lfloor\mathbf{E}_{[n]}\rceil^{\alpha}.\end{aligned} \tag{18}$$

where $\hat{\mathbf{F}}_{[n]}$ is the estimate of $\mathbf{F}_{[n]}$ obtained by using the TDE [24] as follows:

$$\hat{\mathbf{F}}_{[n]} \cong \mathbf{F}_{[n-1]} = \mathbf{Z}_{[n]} - \mathbf{A}_{[n-1]} - \mathbf{B}\,\mathbf{U}_{[n-1]}. \tag{19}$$

The accuracy of the convergence of $\hat{\mathbf{F}}_{[n]}$ to $\mathbf{F}_{[n]}$ depends on how short the sampling time is. Notice that the TDE is well known for its ability to approximate slow-varying and bounded uncertainties in a simple manner without exact knowledge of the controlled plant dynamics. Indeed, this method uses the computed control signals and the available states for measurements one step in the past.

Finally, combining (17) and (18) yields the following control law:

$$\begin{aligned}\mathbf{U}_{[n]} = &\underbrace{-\mathbf{B}^{-1}\left[\mathbf{A}_{[n]} + \hat{\mathbf{F}}_{[n]} - \mathbf{Z}^r_{[n+1]} - \mathbf{\Lambda}_1\mathbf{E}_{[n]} - \mathbf{\Lambda}_2\lfloor\mathbf{E}_{[n]}\rceil^{\alpha}\right]}_{\text{equivalent control}} \\ &-\underbrace{\mathbf{B}^{-1}\left[(\mathbf{I}_4 - T_s\mathbf{L})\mathbf{S}_{[n]} + T_s\left(\mathbf{Q}_1\lfloor\mathbf{S}_{[n]}\rceil^{\gamma_1} + \mathbf{Q}_2\lfloor\mathbf{S}_{[n]}\rceil^{\gamma_2} + \mathbf{Q}_3\lfloor\mathbf{S}_{[n]}\rceil^{0}\right)\right]}_{\text{enhanced PRL}}.\end{aligned} \tag{20}$$

Theorem 1. *Consider a discrete-time nonlinear system of the studied six-phase motor (5). The method proposed in (20) guarantees the convergence of each stator current to its reference in a finite time if the following condition is met for $i = 1, \cdots, 4$:*

$$q_{3i} > f_i, \tag{21}$$

and each stator current tracking error will converge to zero within at most $n^* + 1$ steps, defined as:

$$n^* = \frac{\left|S_{i[0]}\right|}{T_s\,\rho_i - \delta_i}. \tag{22}$$

Proof of Theorem 1. Substituting the control law obtained in (20) into the model dynamics (5) yields:

$$\mathbf{S}_{[n+1]} = \tilde{\mathbf{F}}_{[n]} + (\mathbf{I}_4 - T_s\mathbf{L})\mathbf{S}_{[n]} - T_s\mathbf{Q}_1\lfloor\mathbf{S}_{[n]}\rceil^{\gamma_1} - T_s\mathbf{Q}_2\lfloor\mathbf{S}_{[n]}\rceil^{\gamma_2} - T_s\mathbf{Q}_3\lfloor\mathbf{S}_{[n]}\rceil^{0}, \tag{23}$$

where $\tilde{\mathbf{F}}_{[n]} = \mathbf{F}_{[n]} - \hat{\mathbf{F}}_{[n]} = O(T_s^2)$ denotes the error of the estimation, which verifies for $i = 1, \cdots, 4$ that:

$$\left|\tilde{F}_{i[n]}\right| \leq T_s f_i, \tag{24}$$

where f_i is a known positive constant.

The closed-loop error dynamics in (23) can be divided into four sub-systems:

$$S_{i[n+1]} = \tilde{F}_{i[n]} + (1 - T_s l_i)S_{i[n]} - T_s\left(q_{1i}|S_{i[n]}|^{\gamma_{1i}} + q_{2i}|S_{i[n]}|^{\gamma_{2i}} + q_{3i}\right)\text{sign}\left(S_{i[n]}\right). \tag{25}$$

For this proof, the following rules [11,24] that ensure a quasi-SM should be demonstrated:

$$\begin{cases} S_{i[n]} > \epsilon & \Rightarrow -\epsilon \leq S_{i[n+1]} < S_{i[n]} \\ S_{i[n]} < -\epsilon & \Rightarrow S_{i[n]} < S_{i[n+1]} \leq \epsilon \\ |S_{i[n]}| \leq \epsilon & \Rightarrow \left|S_{i[n+1]}\right| \leq \epsilon \end{cases} \tag{26}$$

where ϵ is a positive-definite quasi-SM bandwidth that is chosen to be equal to $T_s(f_i + q_{3i})$.

1. Let us start with the case where $S_{i[n]} > T_s(f_i + q_{3i}) > 0$. Then:

$$\begin{aligned} S_{i[n+1]} &= \tilde{F}_{i[n]} + (1 - T_s l_i)S_{i[n]} - T_s\left(q_{1i}|S_{i[n]}|^{\gamma_{1i}} + q_{2i}|S_{i[n]}|^{\gamma_{2i}} + q_{3i}\right) \\ S_{i[n+1]} - S_{i[n]} &= \tilde{F}_{i[n]} - T_s l_i S_{i[n]} - T_s\left(q_{1i}|S_{i[n]}|^{\gamma_{1i}} + q_{2i}|S_{i[n]}|^{\gamma_{2i}} + q_{3i}\right). \end{aligned} \tag{27}$$

   Choosing q_{3i} to satisfy (21) ensures that $S_{i[n+1]} - S_{i[n]} < 0 \Rightarrow S_{i[n+1]} < S_{i[n]}$. Otherwise, $-T_s(f_i + q_{3i}) \leq S_{i[n+1]}$ can be expressed as follows:

$$\tilde{F}_{i[n]} + (1 - T_s l_i)S_{i[n]} - T_s\left(q_{1i}|S_{i[n]}|^{\gamma_{1i}} + q_{2i}|S_{i[n]}|^{\gamma_{2i}} + q_{3i}\right) \geq -T_s(f_i + q_{3i}). \tag{28}$$

   Hence:

$$S_{i[n]} \geq \frac{-\left[\tilde{F}_{i[n]} + T_s\left(q_{1i}|S_{i[n]}|^{\gamma_{1i}} + q_{2i}|S_{i[n]}|^{\gamma_{2i}} + f_i\right)\right]}{(1 - T_s l_i)}. \tag{29}$$

   In this case, $S_{i[n]}$ is positive definite, and it is obvious that the right side of the inequality is negative definite, which implies that $-T_s(f_i + q_{3i}) \leq S_{i[n+1]}$ is always true.

2. Now, let us consider the case where $S_{i[n]} < -T_s(f_i + q_{3i}) < 0$. On one hand, let us rewrite the inequality $S_{i[n]} < S_{i[n+1]}$ as:

$$\begin{aligned} S_{i[n]} &< \tilde{F}_{i[n]} + (1 - T_s l_i)S_{i[n]} - T_s\left(q_{1i}|S_{i[n]}|^{\gamma_{1i}} + q_{2i}|S_{i[n]}|^{\gamma_{2i}} + q_{3i}\right) \\ S_{i[n]} &< \frac{\tilde{F}_{i[n]} - T_s\left(q_{1i}|S_{i[n]}|^{\gamma_{1i}} + q_{2i}|S_{i[n]}|^{\gamma_{2i}} + q_{3i}\right)}{T_s l_i}. \end{aligned} \tag{30}$$

   This is always true, since $q_{3i} > f_i$. On the other hand, $S_{i[n+1]} < T_s(f_i + q_{3i})$ can be expressed as follows:

$$\tilde{F}_{i[n]} + (1 - T_s l_i)S_{i[n]} - T_s\left(q_{1i}|S_{i[n]}|^{\gamma_{1i}} + q_{2i}|S_{i[n]}|^{\gamma_{2i}} + q_{3i}\right) < T_s(f_i + q_{3i}). \tag{31}$$

   It is clear that the above inequality is always true because $S_{i[n]} < 0$ and $T_s q_{3i} > \tilde{F}_{i[n]}$.

3. Finally, let us consider the last case, where $\left|S_{i[n]}\right| \leq T_s(f_i + q_{3i})$, then:

a. If $S_{i[n]}$ is positive definite, then this third case becomes:

$$0 < S_{i[n]} < T_s(f_i + q_{3i}), \tag{32}$$

and

$$\begin{aligned} 0 < (1 - T_s l_i) S_{i[n]} &< (1 - T_s l_i) T_s (f_i + q_{3i}) \\ \tilde{F}_{i[n]} - T_s\left(q_{1i}|S_{i[n]}|^{\gamma_{1i}} + q_{2i}|S_{i[n]}|^{\gamma_{2i}} + q_{3i}\right) < S_{i[n+1]} &< (1 - T_s l_i) T_s (f_i + q_{3i}) + \star. \end{aligned} \tag{33}$$

where $\star = \tilde{F}_{i[n]} - T_s\left(q_{1i}|S_{i[n]}|^{\gamma_{1i}} + q_{2i}|S_{i[n]}|^{\gamma_{2i}} + q_{3i}\right)$. Moreover, if (21) is verified, then:

$$\tilde{F}_{i[n]} - T_s\left(q_{1i}|S_{i[n]}|^{\gamma_{1i}} + q_{2i}|S_{i[n]}|^{\gamma_{2i}} + q_{3i}\right) > -T_s(f_i + q_{3i}), \tag{34}$$

and

$$(1 - T_s l_i) T_s (f_i + q_{3i}) + \tilde{F}_{i[n]} - T_s\left(q_{1i}|S_{i[n]}|^{\gamma_{1i}} + q_{2i}|S_{i[n]}|^{\gamma_{2i}} + q_{3i}\right) < T_s(f_i + q_{3i}). \tag{35}$$

This implies that:

$$\begin{aligned} -T_s(f_i + q_{3i}) < S_{i[n+1]} &< T_s(f_i + q_{3i}) \\ \left|S_{i[n+1]}\right| &< T_s(f_i + q_{3i}). \end{aligned} \tag{36}$$

b. if $S_{i[n]}$ is negative definite, then this third case becomes:

$$-T_s(f_i + q_{3i}) < S_{i[n]} < 0. \tag{37}$$

Using the same methodology for $S_{i[n]} > 0$, it can be easily demonstrated that:

$$\left|S_{i[n+1]}\right| < T_s(f_i + q_{3i}). \tag{38}$$

A quasi-SM convergence is guaranteed, since the inequalities in (26) are demonstrated under the condition (21). Hence, the designed enhanced PRL-based DTSMC (20) is stable. The following demonstration by contradiction is used to show the finite-time convergence of the proposed method:

1. Firstly, let us assume that $S_{i[0]}$ and $S_{i[k]}$ are both strictly positive definite and $\text{sign}\left(S_{i[0]}\right) = \text{sign}\left(S_{i[k]}\right) > 0$ for all $k \leq (n^* + 1)$. Then,

$$\begin{aligned} S_{i[1]} &= \tilde{F}_{i[0]} + (1 - T_s l_i) S_{i[0]} - T_s\left(q_{1i}|S_{i[0]}|^{\gamma_{1i}} + q_{2i}|S_{i[0]}|^{\gamma_{2i}} + q_{3i}\right) \\ &\leq \tilde{F}_{i[0]} + S_{i[0]} - T_s\left(q_{1i}|S_{i[0]}|^{\gamma_{1i}} + q_{2i}|S_{i[0]}|^{\gamma_{2i}} + q_{3i}\right) \\ S_{i[2]} &\leq \tilde{F}_{i[1]} + S_{i[1]} - T_s\left(q_{1i}|S_{i[1]}|^{\gamma_{1i}} + q_{2i}|S_{i[1]}|^{\gamma_{2i}} + q_{3i}\right) \\ &\leq \sum_{j=0}^{1} \tilde{F}_{i[j]} + S_{i[0]} - T_s\left(q_{1i}\sum_{j=0}^{1}|S_{i[j]}|^{\gamma_{1i}} + q_{2i}\sum_{j=0}^{1}|S_{i[j]}|^{\gamma_{2i}} + 2q_{3i}\right) \\ &\vdots \\ S_{i[k]} &\leq \sum_{j=0}^{k-1} \tilde{F}_{i[j]} + S_{i[0]} - T_s\left(q_{1i}\sum_{j=0}^{k-1}|S_{i[j]}|^{\gamma_{1i}} + q_{2i}\sum_{j=0}^{k-1}|S_{i[j]}|^{\gamma_{2i}} + kq_{3i}\right) \\ &\leq \sum_{j=0}^{k-1} \tilde{F}_{i[j]} + S_{i[0]} - kT_s q_{3i} \\ &\leq \left|S_{i[0]}\right| + kT_s(f_i - q_{3i}). \end{aligned} \tag{39}$$

Hence, one can notice that n^* ensures that

$$\left|S_{i[0]}\right| + n^* T_s(f_i - q_{3i}) = 0. \tag{40}$$

It follows that:

$$\begin{aligned} S_{i[n^*+1]} &\leq \left|S_{i[0]}\right| + (n^*+1)T_s(f_i - q_{3i}) \\ &< \left|S_{i[0]}\right| + n^* T_s(f_i - q_{3i}) = 0. \end{aligned} \tag{41}$$

which is contradictory to the fact that $S_{i[k]} > 0$, $\forall\, k \leq (n^*+1)$.

2. Secondly, let us assume that $S_{i[0]}$ and $S_{i[k]}$ are both strictly negative definite and $\text{sign}\left(S_{i[0]}\right) = \text{sign}\left(S_{i[k]}\right) < 0$ for all $k \leq (n^*+1)$. Then,

$$\begin{aligned} S_{i[1]} &= \tilde{F}_{i[0]} + (1 - T_s l_i)S_{i[0]} - T_s\left(q_{1i}|S_{i[0]}|^{\gamma_{1i}} + q_{2i}|S_{i[0]}|^{\gamma_{2i}} + q_{3i}\right) \\ &\geq \tilde{F}_{i[0]} + S_{i[0]} - T_s\left(q_{1i}|S_{i[0]}|^{\gamma_{1i}} + q_{2i}|S_{i[0]}|^{\gamma_{2i}} + q_{3i}\right) \\ S_{i[2]} &\geq \tilde{F}_{i[1]} + S_{i[1]} - T_s\left(q_{1i}|S_{i[1]}|^{\gamma_{1i}} + q_{2i}|S_{i[1]}|^{\gamma_{2i}} + q_{3i}\right) \\ &\geq \sum_{j=0}^{1} \tilde{F}_{i[j]} + S_{i[0]} - T_s\left(q_{1i}\sum_{j=0}^{1}|S_{i[j]}|^{\gamma_{1i}} + q_{2i}\sum_{j=0}^{1}|S_{i[j]}|^{\gamma_{2i}} + 2q_{3i}\right) \\ &\vdots \\ S_{i[k]} &\geq \tilde{F}_{i[k-1]} + S_{i[k-1]} - T_s\left(q_{1i}|S_{i[k-1]}|^{\gamma_{1i}} + q_{2i}|S_{i[k-1]}|^{\gamma_{2i}} + q_{3i}\right) \\ &\geq \sum_{j=0}^{k-1} \tilde{F}_{i[j]} + S_{i[0]} - T_s\left(q_{1i}\sum_{j=0}^{k-1}|S_{i[j]}|^{\gamma_{1i}} + q_{2i}\sum_{j=0}^{k-1}|S_{i[j]}|^{\gamma_{2i}} + kq_{3i}\right) \\ &\geq -\left|S_{i[0]}\right| + kT_s(q_{3i} - f_i). \end{aligned} \tag{42}$$

Once again, we can clearly notice that n^* verifies that

$$-\left|S_{i[0]}\right| + kT_s(q_{3i} - f_i) = 0. \tag{43}$$

It follows that

$$\begin{aligned} S_{i[n^*+1]} &\geq -\left|S_{i[0]}\right| + (n^*+1)T_s(q_{3i} - f_i) \\ &> -\left|S_{i[0]}\right| + n^* T_s(q_{3i} - f_i) = 0 \end{aligned} \tag{44}$$

which is contradictory to the fact that $S_{i[k]} < 0$, $\forall\, k \leq (n^*+1)$.

This concludes the proof of Theorem 1. □

4. Experimental Results

The designed enhanced PRL-based DTSMC method was implemented in real time to validate its performance. Figure 3 shows a photograph of the experimental setup employed to validate the proposed controller. On the other hand, Table 1 summarizes the components of the mentioned platform. The DC power that supplied the system provided a constant DC-bus voltage. The two 2L-VSCs were controlled by a dSPACE MABXII DS1401 real-time rapid prototyping platform with Simulink. The identified parameters of the machine are given in Table 2. The control parameters were chosen to satisfy the stability of the closed-loop system, and their tuning was performed heuristically based on a trial-and-error method, obtaining the following values:

$$\mathbf{\Lambda}_1 = \mathbf{\Lambda}_2 = 0.1\,\mathbf{I}_4, \qquad \alpha_1 = \alpha_2 = \alpha_3 = \alpha_4 = 0.8,$$

$$\mathbf{L} = 400\,\mathbf{I}_4, \qquad \mathbf{Q}_1 = \mathbf{Q}_2 = 0.5\,\mathbf{I}_4, \qquad \mathbf{Q}_3 = 0.1\,\mathbf{I}_4,$$
$$\gamma_{11} = \gamma_{12} = \gamma_{13} = \gamma_{14} = 0.8, \qquad \gamma_{21} = \gamma_{22} = \gamma_{23} = \gamma_{24} = 1.35.$$

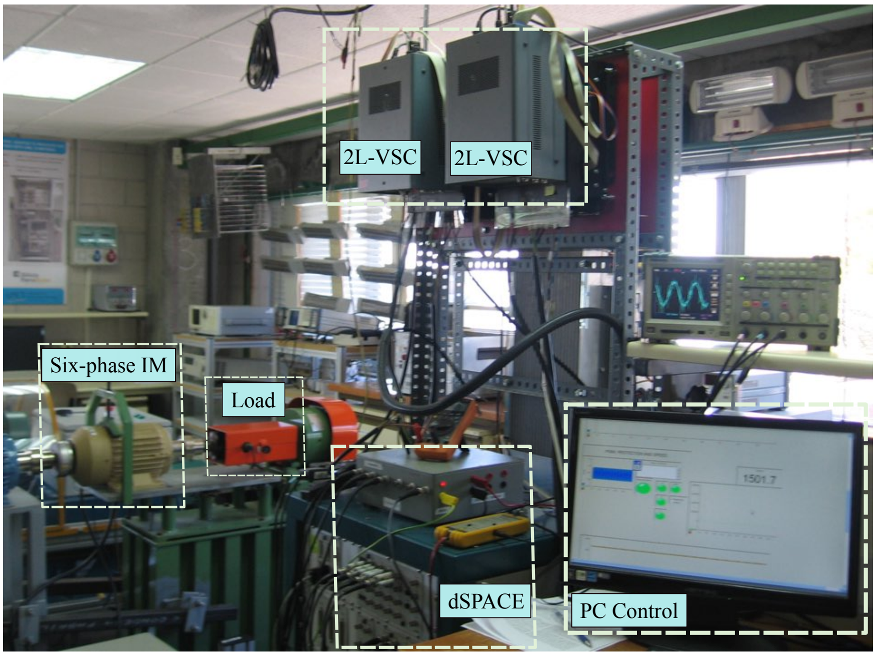

Figure 3. Experimental platform of the six-phase IM control system.

Table 1. Experimental platform's components.

Description	Characteristics
Current sensor	LA 55-P, frequency bandwidth from 0 to 200 kHz
A/D converter	16-bit
Speed sensor	1024 ppr incremental encoder
Variable load	5 HP eddy current brake
Six-phase IM	2 kW

Table 2. Electrical and mechanical parameters of the six-phase IM.

Parameter	Value	Parameter	Value
Rotor resistance	$R_s = 6.7\,\Omega$	Inertia coefficient	$J = 0.07$ kg·m^2
Leakage stator inductance	$L_{ls} = 5.85$ mH	Friction coefficient	$B = 0.0004$ kg·m^2
Mutual inductance	$L_m = 708.5$ mH	DC-link voltage	$V_{\text{dc}} = 400$ V
Rotor inductance	$L_r = 626.8$ mH	Pole pairs	$P = 1$

4.1. Analysis Criteria

The proposed controller was evaluated through the mean squared error (MSE), which was calculated between the reference and measured stator currents. The MSE was determined as follows:

$$\text{MSE}(I_{s\gamma}) = \sqrt{\frac{1}{N}\sum_{n=1}^{N}\left(I^r_{s\gamma[n]} - I_{s\gamma[n]}\right)^2} \tag{45}$$

where $I^r_{s\gamma[n]}$ is the stator current reference and $I_{s\gamma[n]}$ represents the measured stator currents, such as $\gamma \in \{d, q, \alpha, \beta, x, y\}$, while N represents the total number of samples.

4.2. Steady-State Results

The following results were obtained at a sampling frequency of 16 kHz. The eddy current brake was adjusted to generate a q-plane stator current of 1.5 A for the asymmetrical six-phase IM. Two rotor speeds were set: 1000 and 1 500 rpm. Table 3 shows these results, which are presented as the MSEs of the stator currents in $(\alpha - \beta)$, $(x - y)$, and $(d - q)$. The data show the good performance of the proposed controller when applied to the six-phase IM. For comparative purposes, Table 4 presents the same results for a basic DTSMC version proposed in [11]. It can be noticed that the proposed method improved its performance regarding the $\alpha - \beta$ plane.

Table 3. Performance behavior of the stator currents $(\alpha - \beta)$, $(x - y)$, $(d - q)$, and MSE (A) for two different speed conditions (rpm).

		Sampling	**Frequency**	**16 kHz**		
ω_m^r	MSE_α	MSE_β	MSE_x	MSE_y	MSE_d	MSE_q
1000 rpm	0.1595	0.1639	0.2706	0.2808	0.1609	0.1625
1500 rpm	0.1796	0.1827	0.2789	0.2991	0.1741	0.1880

Table 4. Performance behavior of the stator currents $(\alpha - \beta)$, $(x - y)$, $(d - q)$, and MSE (A) for two different speed conditions (rpm) for a basic DTSMC [11].

		Sampling	**Frequency**	**16 kHz**		
ω_m^r	MSE_α	MSE_β	MSE_x	MSE_y	MSE_d	MSE_q
1000 rpm	0.1860	0.1808	0.2032	0.2026	0.1766	0.1860
1500 rpm	0.1655	0.1716	0.1969	0.1999	0.1708	0.1664

At the same time, Figure 4 presents a polar graph of the stator currents for two mechanical speeds (1000 and 1500 rpm). The analysis was performed with a fixed q-plane current reference, and the amplitudes of the $(\alpha - \beta)$ stator currents were the same with different speeds. The graph also shows the$(x - y)$ currents, where it can be noticed that they presented similar behaviors under various speeds. Moreover, the tracking of the $(\alpha - \beta)$ stator currents was excellent, with a low ripple. Finally, Figure 5 shows the same results for the basic DTSMC proposed in [11].

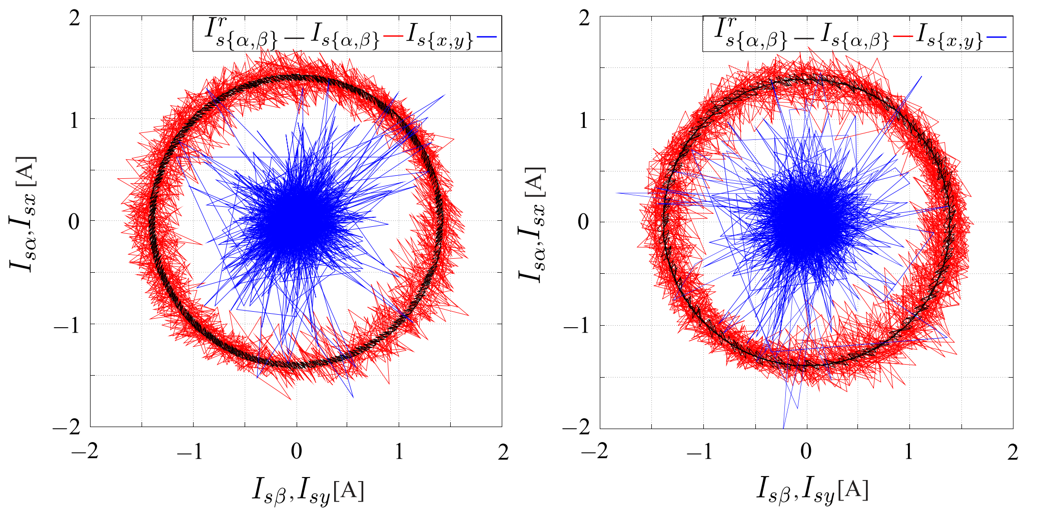

Figure 4. Stator currents for the proposed enhanced PRL-based DTSMC in the $(\alpha - \beta)$ and $(x - y)$ planes for different speed conditions ω_m. Stator currents for the proposed PRL-based DTSMC in the $(\alpha - \beta)$ and $(x - y)$ planes for a speed ω_m of (**left**) 1000 or (**right**) 1500 rpm.

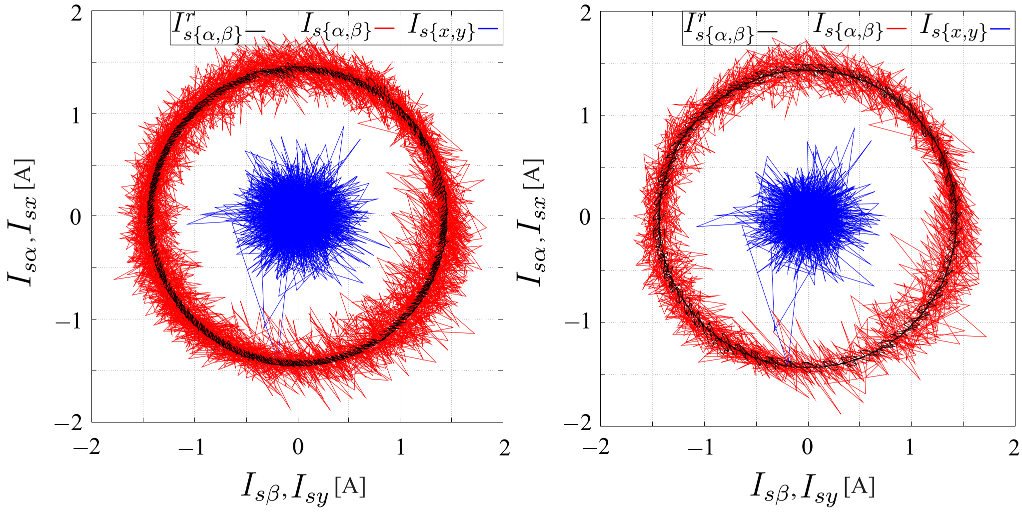

Figure 5. Stator currents in the $(\alpha - \beta)$ and $(x - y)$ planes for different speed conditions ω_m. Stator currents for a basic DTSMC in the $(\alpha - \beta)$ and $(x - y)$ planes for a speed ω_m of (**left**) 1000 or (**right**) 1500 rpm.

4.3. Transient Condition Results

Then, a transient condition, which was defined by a step modification in the q-plane stator current reference (I^r_{sq}) produced by the reversal condition (1000 to −500 rpm), was executed. Figure 6 shows the test and compares it with that of the basic DTSMC version proposed in [11], where a settling time of approximately 2 ms and an overshoot of 28% were identified, confirming a speedy and smooth dynamic response in comparison to that of the basic version, with a settling time of 2 ms and an overshoot of 68%.

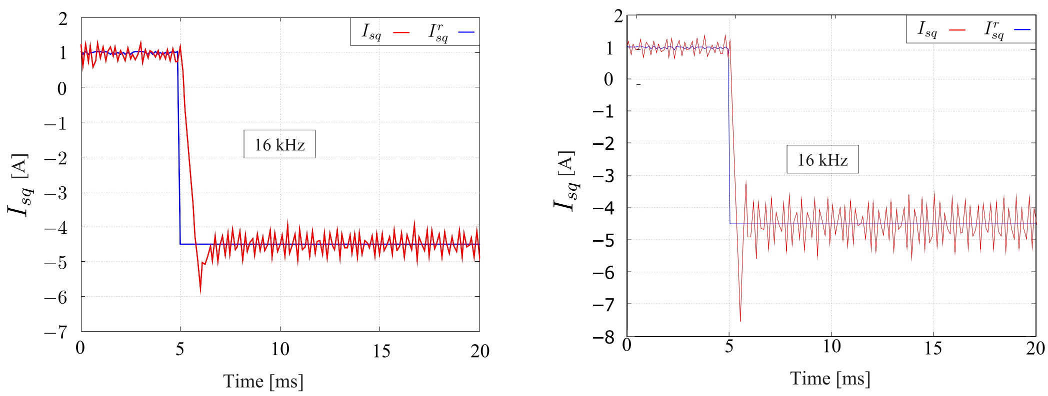

Figure 6. Transient condition of the q-plane current of a speed reversal action from 1000 to −500 rpm from ω_m at a sampling frequency of 16 kHz. Transient condition of the q-plane current of a speed reversal action from 1000 to −500 rpm from ω_m at a sampling frequency of 16 kHz for the proposed controller (**left**) and a basic DTSMC version (**right**).

Two reversal tests were performed to analyze the dynamic behavior of the proposed current controller. Figure 7 presents the results obtained when the speed was varied from −500 to 1000 rpm and from 1000 to −500 rpm. We could verify the proper performance of the current tracking.

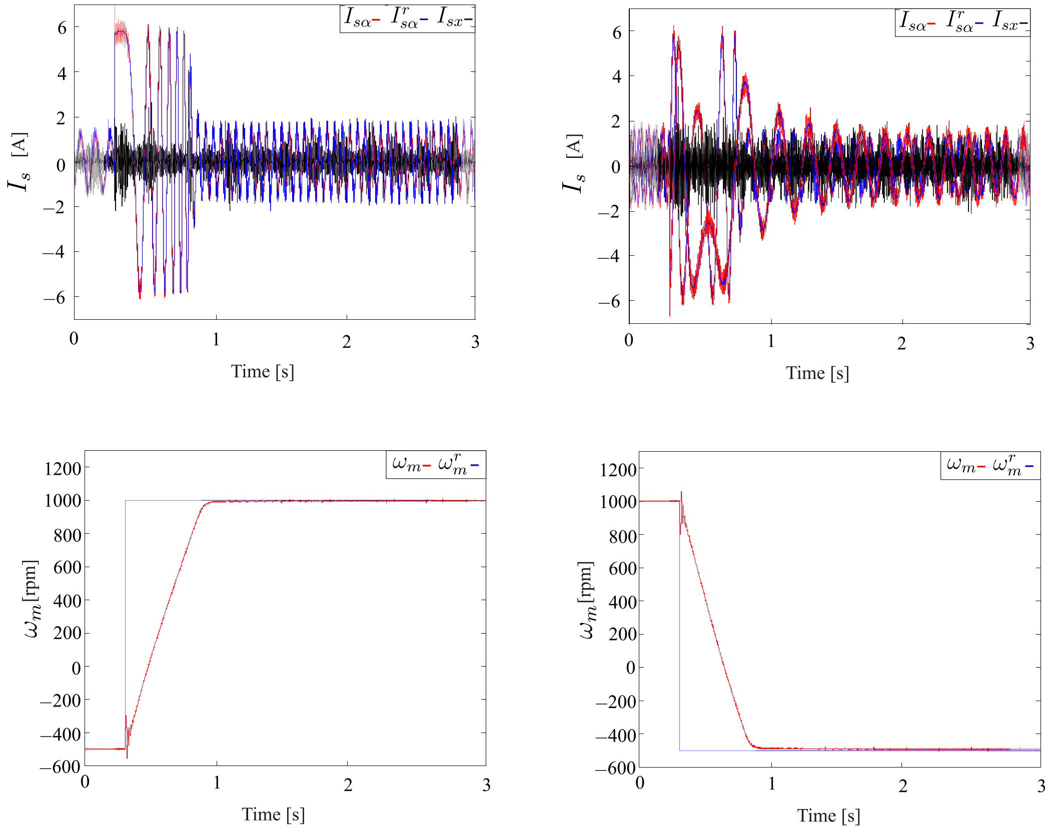

Figure 7. Transient behavior of stator currents of a speed reversal action from ω_m. The first results are from -500 to 1000 rpm, and then from 1000 to -500 rpm.

4.4. Parameter Mismatch Analysis

For the mismatch analysis, the controller performance was verified with a change in L_m of 25% of the nominal value to quantify the robustness to uncertainties. The results show that the performance was practically the same at both rotor speeds, offering outstanding robustness. The MSE values for this particular test are presented in Table 5. Note that the variation in L_m implies a variation in the whole system dynamic, since $\mathbf{A}_{[n]}$ and $\mathbf{B}$ are in terms of this inductance [25,26].

Table 5. Performance behavior of the stator currents $(\alpha - \beta)$, $(x - y)$, $(d - q)$, and MSE (A) for two different speed conditions (rpm) with a variation in L_m.

		Sampling	**Frequency**	**16 kHz**		
ω_m^r	MSE_α	MSE_β	MSE_x	MSE_y	MSE_d	MSE_q
1000	0.1703	0.1696	0.2937	0.3130	0.1669	0.1729
1500	0.1855	0.1894	0.2742	0.3005	0.1797	0.1950

Finally, a change in R_r was also made to check the side effects on the system. As R_r had less of an impact on the model, the current control variation was insignificant. However, the speed control response time tended to slightly increase due to the estimation of the τ_r parameter, as shown in Figure 8.

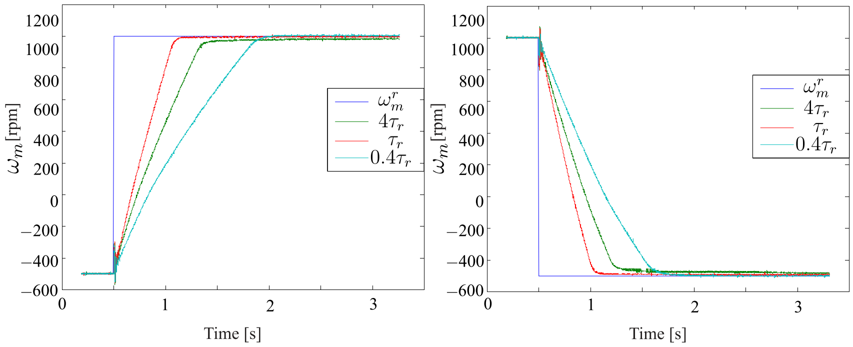

Figure 8. Transient behavior of a speed reversal action from ω_m. The first results are from -500 to 1000 rpm, and then from 1000 to -500 rpm, with different values of τ_r.

5. Conclusions

This paper presented an inner robust enhanced reaching-law-based DTSMC for controlling the stator currents in the $(\alpha - \beta)$ and $(x - y)$ planes of a six-phase IM with an outer PI rotor speed loop. The proposed method uses a discrete terminal sliding manifold to enhance the convergence speed when the system's trajectories are far from the equilibrium point. Moreover, this technique is based on an enhanced reaching law that combines Gao's reaching law and the exponential-based bi-power reaching law to ensure a faster reaching rate in a small quasi-sliding mode band while reducing the chattering phenomenon. Otherwise, the developed discrete-time approach estimates the bounded uncertainties and unmeasurable rotor currents via the TDE method for a better control effort and improved tracking performance. Based on the results, the proposed technique showed optimal behavior in current tracking with a low mean square error. Compared with previous sliding-mode-based controllers, the proposed controller also ensures robustness, as demonstrated by the error tracking in parameter mismatch tests. However, it delivers a higher speed of convergence and smoother dynamics in settling time, overshoot, and faster convergence in all operating conditions. Therefore, the enhanced PRL-based DTSMC can be an excellent option for different rotor conditions in industrial applications. This paper demonstrated that, with modifications, SMC can include more power terms to reduce chattering. Moreover, the good performance of the proposed controller gave the motivation to address an exhaustive comparison of the proposed methods against others, such as field-oriented control, direct torque control, and/or FCS-MPC, as a near-future research topic. Moreover, this paper opens the door for a niche of applications of other nonlinear control techniques, such as higher-order SMC, fuzzy logic, and backstepping.

Author Contributions: Conceptualization, Y.K. and J.R.; methodology, Y.K. and J.R.; software, Y.K., J.R. and J.D.-G.; validation, J.D.-G.; formal analysis, Y.K., J.R., J.D.-G., M.A. and O.G.; investigation, Y.K., J.R. and J.D.-G.; resources, J.D.-G.; data curation, M.A. and O.G.; writing—original draft preparation, Y.K., J.R., M.A. and O.G.; writing—review and editing, Y.K., J.R., M.A. and O.G.; visualization, Y.K. and J.R.; supervision, J.R.; project administration, J.D.-G.; funding acquisition, J.D.-G. All authors have read and agreed to the published version of the manuscript.

Funding: This research received no external funding.

Data Availability Statement: Not applicable.

Acknowledgments: J.R. acknowledges the Guest Editor for the invitation (waiver) for this paper. J.R., M.A., and O.G. also acknowledge the support of CONACYT through its PRONII program.

Conflicts of Interest: The authors declare no conflict of interest.

Abbreviations

The following abbreviations are used in this manuscript:

2L-VSC	Two-level voltage course converter
IM	Induction motor
DSMC	Discrete-time sliding mode control
DTSMC	Discrete-time terminal sliding mode control
ERL	Exponential reaching law
FCS-MPC	Finite-control-set MPC
MPC	Model predictive control
MSE	Mean squared error
PI	Proportional–integral
PC	Personal computer
PRL	Power-reaching law
TDE	Time delay estimation
TSM	Terminal sliding mode
SMC	Sliding mode control

References

1. Gonzalez, O.; Ayala, M.; Romero, C.; Delorme, L.; Rodas, J.; Gregor, R.; Gonzalez-Prieto, I.; Durán, M.J. Model Predictive Current Control of Six-Phase Induction Motor Drives Using Virtual Vectors and Space Vector Modulation. *IEEE Trans. Power Electron.* **2022**, *37*, 7617–7628. [CrossRef]
2. Salem, A.; Narimani, M. A Review on Multiphase Drives for Automotive Traction Applications. *IEEE Trans. Transp. Electrif.* **2019**, *5*, 1329–1348. [CrossRef]
3. Pantea, A.; Yazidi, A.; Betin, F.; Carrière, S.; Sivert, A.; Vacossin, B.; Henao, H.; Capolino, G.A. Fault-Tolerant Control of a Low-Speed Six-Phase Induction Generator for Wind Turbines. *IEEE Trans. Ind. Appl.* **2019**, *55*, 426–436. [CrossRef]
4. Levi, E. Advances in Converter Control and Innovative Exploitation of Additional Degrees of Freedom for Multiphase Machines. *IEEE Trans. Ind. Electron.* **2016**, *63*, 433–448. [CrossRef]
5. Liu, Z.; Li, Y.; Zheng, Z. A review of drive techniques for multiphase machines. *CES Trans. Electr. Mach. Syst.* **2018**, *2*, 243–251. [CrossRef]
6. Rodas, J.; Gonzalez-Prieto, I.; Kali, Y.; Saad, M.; Doval-Gandoy, J. Recent Advances in Model Predictive and Sliding Mode Current Control Techniques of Multiphase Induction Machines. *Front. Energy Res.* **2021**, *9*, 729034 . [CrossRef]
7. Rodas, J. A Brief Survey of Model Predictive Current Control Techniques for Six-Phase Induction Machines. In Proceedings of the 2021 IEEE CHILEAN Conference on Electrical, Electronics Engineering, Information and Communication Technologies (CHILECON), Valparaiso, Chile, 6–9 December 2021; pp. 1–6. [CrossRef]
8. Gonçalves, P.; Cruz, S.; Mendes, A. Finite Control Set Model Predictive Control of Six-Phase Asymmetrical Machines—An Overview. *Energies* **2019**, *12*, 4693. [CrossRef]
9. Duran, M.; Gonzalez-Prieto, I.; Gonzalez-Prieto, A.; Aciego, J.J. The Evolution of Model Predictive Control in Multiphase Electric Drives: A Growing Field of Research. *IEEE Ind. Electron. Mag.* **2022**, *16*, 29–39. . [CrossRef]
10. Habib, A.; Shawier, A.; Mamdouh, M.; Samy Abdel-Khalik, A.; Hamad, M.S.; Ahmed, S. Predictive current control based pseudo six-phase induction motor drive. *Alex. Eng. J.* **2022**, *61*, 3937–3948. [CrossRef]
11. Kali, Y.; Ayala, M.; Rodas, J.; Saad, M.; Doval-Gandoy, J.; Gregor, R.; Benjelloun, K. Current Control of a Six-Phase Induction Machine Drive Based on Discrete-Time Sliding Mode with Time Delay Estimation. *Energies* **2019**, *12*, 170. [CrossRef]
12. Kali, Y.; Saad, M.; Doval-Gandoy, J.; Rodas, J.; Benjelloun, K. Discrete sliding mode control based on exponential reaching law and time delay estimation for an asymmetrical six-phase induction machine drive. *IET Electr. Power Appl.* **2019**, *13*, 1660–1671. [CrossRef]
13. Latosiński, P. Sliding mode control based on the reaching law approach—A brief survey. In Proceedings of the 2017 22nd International Conference on Methods and Models in Automation and Robotics (MMAR), Miedzyzdroje, Poland, 28–31 August 2017; pp. 519–524. [CrossRef]
14. Ma, H.; Wu, J.; Xiong, Z. A Novel Exponential Reaching Law of Discrete-Time Sliding-Mode Control. *IEEE Trans. Ind. Electron.* **2017**, *64*, 3840–3850. [CrossRef]
15. Ma, H.; Li, Y.; Xiong, Z. Discrete-Time Sliding-Mode Control with Enhanced Power Reaching Law. *IEEE Trans. Ind. Electron.* **2019**, *66*, 4629–4638. [CrossRef]
16. Gao, W.; Wang, Y.; Homaifa, A. Discrete-time variable structure control systems. *IEEE Trans. Ind. Electron.* **1995**, *42*, 117–122. [CrossRef]
17. Zheng, L.; Jiang, F.; Song, J.; Gao, Y.; Tian, M. A Discrete-Time Repetitive Sliding Mode Control for Voltage Source Inverters. *IEEE J. Emerg. Sel. Top. Power Electron.* **2018**, *6*, 1553–1566. [CrossRef]
18. Kali, Y.; Ayala, M.; Rodas, J.; Saad, M.; Doval-Gandoy, J.; Gregor, R.; Benjelloun, K. Time Delay Estimation Based Discrete-Time Super-Twisting Current Control for a Six-Phase Induction Motor. *IEEE Trans. Power Electron.* **2020**, *35*, 12570–12580. [CrossRef]

19. Kali, Y.; Saad, M.; Doval-Gandoy, J.; Rodas, J. Discrete Terminal Super-Twisting Current Control of a Six-Phase Induction Motor. *Energies* **2021**, *14*, 1339. [CrossRef]
20. Du, H.; Chen, X.; Wen, G.; Yu, X.; Lü, J. Discrete-Time Fast Terminal Sliding Mode Control for Permanent Magnet Linear Motor. *IEEE Trans. Ind. Electron.* **2018**, *65*, 9916–9927. [CrossRef]
21. Xiong, X.; Chu, Y.; Udai, A.D.; Kamal, S.; Jin, S.; Lou, Y. Implicit Discrete-Time Terminal Sliding Mode Control for Second-Order Systems. *IEEE Trans. Circuits Syst. II Express Briefs* **2021**, *68*, 2508–2512. [CrossRef]
22. Wang, Y.; Jiang, S.; Chen, B.; Wu, H. Trajectory Tracking Control of Underwater Vehicle-Manipulator System Using Discrete Time Delay Estimation. *IEEE Access* **2017**, *5*, 7435–7443. [CrossRef]
23. Levi, E. Power Electronics and Motor Drives, Chapter: FOC: Field Oriented Control, United States. In *The Industrial Electronics Handbook*, 2nd. ed.; CRC Press: Boca Raton, FL, USA, 2011.
24. Kali, Y.; Saad, M.; Benjelloun, K.; Fatemi, A. Discrete-time second order sliding mode with time delay control for uncertain robot manipulators. *Robot. Auton. Syst.* **2017**, *94*, 53–60. [CrossRef]
25. Delorme, L.; Ayala, M.; Rodas, J.; Gregor, R.; Gonzalez, O.; Doval-Gandoy, J. Comparison of the Effects on Stator Currents Between Continuous Model and Discrete Model of the Three-phase Induction Motor in the Presence of Electrical Parameter Variations. In Proceedings of the 2020 IEEE International Conference on Industrial Technology (ICIT), Buenos Aires, Argentina, 26–28 February 2020; pp. 151–156. [CrossRef]
26. Bermudez, M.; Arahal, M.R.; Duran, M.J.; Gonzalez-Prieto, I. Model predictive control of six-phase electric drives including ARX disturbance estimator. *IEEE Trans. Ind. Electron.* **2020**, *68*, 81–91. [CrossRef]